

# Magnetorotational Instability in Electrically Driven Flow of Liquid Metal: Spectral Analysis

*I.V.Khalzov<sup>1,2</sup>, A.I.Smolyakov<sup>1,2</sup>, V.I.Ilgisonis<sup>1</sup>*

<sup>1</sup>Russian Research Center "Kurchatov Institute", 1 Kurchatov Sq.,  
Moscow, 123182, Russia

<sup>2</sup>University of Saskatchewan, 116 Science Place, Saskatoon, SK, S7N5E2,  
Canada

## Abstract

The spectral stability of liquid metal differentially rotating in transverse magnetic field is studied numerically by solving the eigenvalue problem with rigid-wall boundary conditions. The equilibrium velocity profile used in calculations corresponds to the electrically driven flow in circular channel with the rotation law  $\Omega(r) \propto 1/r^2$ . This type of flow profile is planned to be used in new experimental device to test the magnetorotational instability (MRI) in laboratory. Our analysis includes calculations of the eigen-frequency spectra for both axisymmetric and non-axisymmetric modes. It is found that for chosen device parameters the flow is always spectrally unstable due to MRI with the fastest growth rate corresponding to the axisymmetric mode.

## 1 Introduction

Magnetorotational instability (MRI) – the instability of conducting fluid, rotating in magnetic field – is one of the most important processes in astrophysics. MRI is believed to be responsible for angular momentum transport in such objects as accretion disks formed around massive black holes and active galactic nuclei. This instability was originally discovered in 1959 by Velikhov [1], who, though, did not consider it in an astrophysical context. It was suggested only in 1991 [2] that a weak magnetic field can linearly destabilize the otherwise stable accretion disk thus directly leading to disk turbulence and orbital angular momentum transport. MRI becomes operative when the angular velocity decreases outwards,  $d\Omega/dr < 0$ , which holds for Keplerian flow in accretion disks ( $\Omega \propto r^{-3/2}$ ).

Because of its importance in understanding of accretion disk physics, a number of experiments have been proposed recently [3]-[8] to study this instability in the laboratory. In most of them a Couette flow of liquid metal between two rotating cylinders placed in external magnetic field is supposed to be used. However this simple design has its disadvantages. The main one

is that the equilibrium flow is controlled almost entirely by the endcaps of the vessel – so-called Ekman effect [9]. In this case the velocity profile is significantly different from Couette flow, so the conditions for MRI may not be met.

Another way to rotate liquid metal is to apply radial electric current between cylinders placed in vertical magnetic field, that produces a Lorentz force driving metal. It is worthwhile noting that in this case the effect of the Ekman layers at the top and bottom insulating caps is considerably reduced. Actually one has to take into account only Hartmann layers which are very small for large Hartmann numbers and do not affect the main body of the flow. This idea was proposed in Russian Research Center "Kurchatov Institute" by E. P. Velikhov (2004, private communication) and the experimental device is being designed there. A similar setup using the plasma instead of liquid metal has been developed in Los Alamos [7].

In this paper we present a linear stability analysis of the electrically driven liquid metal flow in the circular channel for the configuration relevant to Kurchatov experiment. It has been shown in [10] that in the stationary state the angular velocity profile of such flow scales with radius as  $\Omega \propto 1/r^2$  virtually throughout the entire channel cross section if the Hartmann number is large enough ( $Ha \gg 1$ ). This dependence is a particular case of the more general ones,  $\Omega = a + b/r^2$  (Couette flow) and  $\Omega \propto r^{-q}$  (with  $q = 3/2$  corresponding to Keplerian flow) whose stability has been studied analytically and numerically in numerous papers. Therefore some results obtained in those papers are relevant to our study. Let us briefly review them.

Originally MRI was discovered as a powerful local axisymmetric (with azimuthal wave-number  $m = 0$ ) instability [1, 2]. Consideration of non-axisymmetric modes ( $m \neq 0$ ) in local approach (for example, [11]) has shown that these modes become stabilized with increasing values of  $m$ .

Importance of global modes and boundary conditions for MRI problem have been first analyzed in [12]. In [13] authors considered in details non-axisymmetric global modes with free boundary conditions which are not appropriate for the system with rigid walls.

A great deal of work in global stability study of magnetized Couette flow (including our case with  $a = 0$ ) in the frame of non-ideal magnetohydrodynamics (MHD) has been done by Rüdiger et al. (see, for example, [3], [6] and [14]). They found marginal stability for different parameters of the system, but they did not analyze the growth rate of MRI and its dependence on azimuthal wave-number  $m$ .

The goal of this paper is the global spectral stability analysis of the incompressible MHD flow with angular velocity profile  $\Omega \propto 1/r^2$ . The eigen-

value problem for this configuration is set up in Section 2. The main body of results were obtained numerically and are presented in Sections 3, 4, 5. In Section 3 axisymmetric modes ( $m = 0$ ) are considered and their classification according to radial wave-number is made. Section 4 deals with non-axisymmetric modes ( $m \neq 0$ ), the dependence of MRI growth rates on azimuthal  $m$  and axial  $k$  wave-numbers is presented there. In Section 5 we study marginal stability of the system under consideration. In Section 6 we discuss the possibility of MRI in electrically driven liquid metal flow.

## 2 Statement of the Problem

We consider the following model of the experimental device proposed in Kurchatov Institute (Fig. 1). A liquid metal (Sodium) occupying a circular channel is driven by applying uniform vertical magnetic field  $\mathbf{B}_0$  and radial electric current  $I_0$ . The stationary state of this configuration has been studied in details in [10]. It has been shown that in the cylindrical system of coordinates  $(r, \varphi, z)$  the fluid rotates around the  $z$ -axis with the angular velocity, which has the form

$$\Omega(r) = \frac{I_0}{4\pi r^2 \sqrt{\sigma \rho \nu}} \quad (1)$$

almost entirely in the channel if the Hartmann number is large ( $\text{Ha} \gg 1$ ).

Despite the fact that the value of stationary velocity is determined by the dissipative effects (conductivity  $\sigma$  and viscosity  $\nu$  of the fluid) in our study we neglect all of them and assume that the liquid metal is a perfectly conducting, ideal, incompressible fluid with constant density  $\rho$ . These assumptions are valid for the flow with high Reynolds and magnetic Reynolds numbers – such situation takes place in the system under consideration. The model in this case is simplified considerably without removal any essential physical features. Also we note the paper [15] where the calculations of marginal stability for both viscous and inviscid fluids in the case of Couette flow are presented and they are shown to be almost identical.

The fluid dynamics in our model is described by the equations of ideal incompressible MHD:

$$\frac{\partial \mathbf{V}}{\partial t} + (\mathbf{V} \cdot \nabla) \mathbf{V} = -\nabla P + \frac{1}{4\pi\rho} (\mathbf{B} \cdot \nabla) \mathbf{B}, \quad (2)$$

$$\nabla \cdot \mathbf{V} = 0, \quad (3)$$

$$\frac{\partial \mathbf{B}}{\partial t} = \nabla \times [\mathbf{V} \times \mathbf{B}], \quad (4)$$

$$\nabla \cdot \mathbf{B} = 0, \quad (5)$$

where  $P = (p + \mathbf{B} \cdot \mathbf{B}/8\pi)/\rho$  is the normalized total pressure. In equilibrium state ( $\partial/\partial t \rightarrow 0$ ) the fluid, placed in uniform magnetic field  $\mathbf{B}_0 = B_0 \mathbf{e}_z$ , rotates differentially with velocity  $\mathbf{V}_0 = r\Omega(r)\mathbf{e}_\varphi$ . In general, the function  $\Omega(r)$  is arbitrary, since equilibrium can always be maintained by a radial pressure gradient, but we will consider here only the form of  $\Omega(r)$  defined in equation (1).

For the purpose of linear stability analysis, it is advantageous to use a Lagrangian representation. We linearize the equations (2)-(5) near the equilibrium state and introduce the displacement vector  $\boldsymbol{\xi}$ , which is considered to be a small quantity. The perturbations of velocity and magnetic field are then expressed in linear approximation as follows [16]:

$$\delta \mathbf{V} = \frac{\partial \boldsymbol{\xi}}{\partial t} + (\mathbf{V}_0 \cdot \nabla) \boldsymbol{\xi} - (\boldsymbol{\xi} \cdot \nabla) \mathbf{V}_0, \quad (6)$$

$$\delta \mathbf{B} = \nabla \times [\boldsymbol{\xi} \times \mathbf{B}_0]. \quad (7)$$

The linearized dynamics of  $\boldsymbol{\xi}$  is obtained from equation (2):

$$\begin{aligned} \frac{\partial^2 \boldsymbol{\xi}}{\partial t^2} + 2(\mathbf{V}_0 \cdot \nabla) \frac{\partial \boldsymbol{\xi}}{\partial t} + (\mathbf{V}_0 \cdot \nabla)^2 \boldsymbol{\xi} - (\boldsymbol{\xi} \cdot \nabla)(\mathbf{V}_0 \cdot \nabla) \mathbf{V}_0 &= \\ = -\nabla \delta P + \frac{1}{4\pi\rho} (\delta \mathbf{B} \cdot \nabla) \mathbf{B}_0 + \frac{1}{4\pi\rho} (\mathbf{B}_0 \cdot \nabla) \delta \mathbf{B}. \end{aligned} \quad (8)$$

Besides, the equation (3) gives:

$$\nabla \cdot \boldsymbol{\xi} = 0. \quad (9)$$

The normal mode solutions to the system (8)-(9) can be sought in the form:

$$\boldsymbol{\xi}(r, \phi, z, t) = \boldsymbol{\xi}(r) e^{i(m\phi + kz - \omega t)}, \quad (10)$$

$$\delta P(r, \phi, z, t) = \delta P(r) e^{i(m\phi + kz - \omega t)}, \quad (11)$$

where  $m$  (integer) and  $k$  are the azimuthal and axial wave-numbers, respectively, and  $\omega$  is the eigen-frequency. Since normal modes (10), (11) are generally complex, to find the perturbations of physical quantities one has to take either real or imaginary parts of righthand sides in equations (6), (7) and (11).

Substituting the normal mode representation (10) into equations (6) and (7) we find the perturbations:

$$\delta \mathbf{V} = -i\bar{\omega}\boldsymbol{\xi} - \frac{\partial\Omega}{\partial r}\xi_r\mathbf{e}_\varphi, \quad (12)$$

$$\delta \mathbf{B} = ikB_0\boldsymbol{\xi}, \quad (13)$$

while the system (8)-(9) can be rewritten as

$$(\omega_A^2 - \bar{\omega}^2)\xi_r + 2i\Omega\bar{\omega}\xi_\varphi + 2\Omega\frac{\partial\Omega}{\partial r}\xi_r = -\frac{\partial(\delta P)}{\partial r}, \quad (14)$$

$$(\omega_A^2 - \bar{\omega}^2)\xi_\varphi - 2i\Omega\bar{\omega}\xi_r = -\frac{im}{r}\delta P, \quad (15)$$

$$(\omega_A^2 - \bar{\omega}^2)\xi_z = -ik\delta P, \quad (16)$$

$$\frac{1}{r}\frac{\partial(r\xi_r)}{\partial r} + \frac{im}{r}\xi_\varphi + ik\xi_z = 0, \quad (17)$$

where we have introduced the shifted eigen-frequency,

$$\bar{\omega} = \omega - m\Omega,$$

and the Alfvén frequency,

$$\omega_A = kv_A = \frac{kB_0}{\sqrt{4\pi\rho}}.$$

The analogous derivation for more general case including toroidal magnetic field is given by [17].

For computational convenience we introduce dimensionless quantities, taking as a unit of length the radius of the inner cylindrical boundary  $r_1$  and as a unit of frequency the angular velocity at this radius  $\Omega_1$ . Then we have:

$$\begin{aligned} \tilde{r} &= \frac{r}{r_1}, \quad \tilde{r}_1 = 1, \quad \tilde{r}_2 = \frac{r_2}{r_1}, \quad \tilde{h} = \frac{h}{r_1}, \quad \tilde{k} = kr_1, \\ \tilde{v}_A &= \frac{v_A}{r_1\Omega_1}, \quad \tilde{\omega} = \frac{\omega}{\Omega_1}, \quad \tilde{\omega}_A = \frac{\omega_A}{\Omega_1} = \tilde{k}\tilde{v}_A, \quad \tilde{\Omega}(\tilde{r}) = \frac{1}{\tilde{r}^2}, \end{aligned}$$

where  $r_2$  is the radius of the outer cylindrical boundary. In the following consideration we will omit tildes to simplify notations.

The system (14)-(17) can be reduced to one differential equation which in non-dimensional terms is:

$$\begin{aligned} \left[ \frac{(\bar{\omega}^2 - \omega_A^2)xu'}{m^2 + k^2x} \right]' + u \left[ -\frac{\bar{\omega}^2 - \omega_A^2}{4x} + \frac{m\bar{\omega}}{m^2 + k^2x} \left( \Omega' - \frac{k^2\Omega}{m^2 + k^2x} \right) + \right. \\ \left. + \frac{k^2\omega_A^2\Omega^2}{(m^2 + k^2x)(\bar{\omega}^2 - \omega_A^2)} + \frac{k^2\Omega(x\Omega' + \Omega)}{m^2 + k^2x} \right] = 0, \quad (18) \end{aligned}$$

where  $u = r\xi_r$ ,  $x = r^2$  and the prime denotes the derivative with respect to  $x$ . The further reduction of equation (18) is possible if the function  $\Omega(r)$  of the form (1) is used. In this case  $\Omega \propto 1/r^2 \propto 1/x$  and the last term in the equation is zero.

Since we consider the channel with rigid walls the velocity components which are perpendicular to the boundary should vanish at that boundary. It gives us the following boundary conditions

$$u(x_1) = u(x_2) = 0, \quad (19)$$

where  $x_1$  and  $x_2$  correspond to inner  $r_1$  and outer  $r_2$  cylindrical boundaries respectively. Besides, we have to quantize axial wave-number  $k$  appropriately, namely,

$$k = \frac{\pi n_z}{h}, \quad (20)$$

where  $n_z$  is integer and  $h$  is the height of the channel.

The equation (18) with boundary conditions (19) constitutes an eigenvalue problem. The primary objective of our stability study is to determine the spectrum of eigen-frequencies  $\omega$  which has to be found as a part of the solution. Analyzing this eigenvalue problem one can conclude that its solution (and eigen-frequency spectrum as well) depends on five parameters: three wave-numbers – azimuthal  $m$ , axial  $k$  and radial  $n_r$  (it will be introduced later), geometrical factor  $x_2$  and dimensionless Alfvén velocity  $v_A$ . In this work we will focus on study of the dependencies of eigen-frequencies  $\omega$  on wave-numbers  $m$ ,  $k$  and  $n_r$ .

To solve the equation (18) subject to the boundary conditions (19) we used a standard shooting method adapted for eigenvalue problem. For fixed values of problem parameters this method allows one to find the eigenfunctions  $u(x)$  and corresponding eigen-frequencies  $\omega$ . We have performed calculations for the parameters of the experimental device proposed in Kurchatov Institute (see Table 1). In numerical calculations the convenient normalization of eigen-function  $u'(x_1) = 1$  has been chosen. The following sections represent the results of our calculations.

### 3 Axisymmetric Perturbations, $m = 0$

In the axisymmetric case with  $\Omega(x) = 1/x$ , equation (18) is reduced to

$$u'' + k^2 u \left[ -\frac{1}{4x} + \frac{\omega_A^2}{x^3(\omega^2 - \omega_A^2)^2} \right] = 0. \quad (21)$$

Table 1: Parameters of experimental device.

Parameter	Value	Dimensionless Value
Inner radius, $r_1$	3 cm	1
Outer radius, $r_2$	15 cm	5
Height, $h$	6 cm	2
Velocity at inner radius, $v_1$	32 m s <sup>-1</sup>	1
Alfven velocity, $v_A$	8 m s <sup>-1</sup>	0.25

Multiplying this equation by complex conjugate  $u^*$  and integrating over the interval  $[x_1, x_2]$  we obtain the following variational form

$$\int_{x_1}^{x_2} \left[ -|u'|^2 - \frac{k^2}{4x}|u|^2 + \frac{k^2\omega_A^2}{x^3(\omega^2 - \omega_A^2)^2}|u|^2 \right] dx = 0. \quad (22)$$

Some conclusions can be made from its consideration:

1. The expression  $(\omega^2 - \omega_A^2)^2 = \alpha^4$  is a real positive number. Therefore,  $\omega^2 = \omega_A^2 \pm \alpha^2$  is real and eigen-frequencies  $\omega$  are either pure real or pure imaginary.
2. Eigen-frequency spectrum is symmetric with respect to both axis in the complex  $\omega$ -plane.
3. Eigen-functions  $u$  can always be chosen to be real.
4. There is a degeneracy: each eigen-function  $u$  corresponds to four eigen-frequencies  $\omega$ . Two of them are always real,  $\omega = \pm\sqrt{\omega_A^2 + \alpha^2}$ , which means stability. Two others can be imaginary,  $\omega = \pm\sqrt{\omega_A^2 - \alpha^2}$ , which means instability. This instability is known as the axisymmetric magnetorotational instability (MRI of axisymmetric modes).

Besides the azimuthal and axial wave-numbers,  $m$  and  $k$ , to describe eigen-frequencies completely we have to introduce the radial wave-number  $n_r$  which is defined in the case  $m = 0$  as a number of zeros of corresponding real eigen-function. The eigen-spectrum can be represented now by the formal disperse relation  $\omega = \omega(m, k, n_r)$  which relates each set of wave-numbers  $(m, k, n_r)$  with values of eigen-frequencies  $\omega$ .

For  $m = 0$  and lowest axial wave-number  $k = \pi/2$  ( $n_z = 1$ ) the spectrum of eigen-frequencies is shown in figure 2. As one can see, there is a pure imaginary eigen-frequency in the upper half-plane which corresponds to magneto-rotational instability. Also the spectrum has two accumulation

points at  $\omega = \pm\omega_A$  (Alfven resonances). With approaching these points the radial wave-number increases, i. e. the corresponding eigen-functions become oscillating. In this limit the WKB approximation to the equation (21) works well (see, for example, [12]).

Eigen-spectrum shown in figure 2 is formed from coupled Alfven and slow magnetosonic modes. Unlike [18] we did not obtain the fast magnetosonic modes since our consideration is restricted by incompressible MHD model.

It should be noted here that the Alfven resonance lines,  $\text{Re } \omega = \pm\omega_A$ , divide the complex  $\omega$ -plane into 3 regions: 1)  $\text{Re } \omega < -\omega_A$ , 2)  $-\omega_A < \text{Re } \omega < \omega_A$ , and 3)  $\text{Re } \omega > \omega_A$ . The "outer" modes belonging to regions 1 and 3 are always stable (the corresponding eigen-frequencies are real). The unstable modes can emerge only in the central region 2 as a result of coupling of originally stable "inner" modes. As we will show this tendency is valid for non-axisymmetric modes as well.

In figure 3 the samples of axisymmetric eigen-functions with different radial wave-numbers  $n_r$  are shown. No conclusion about localization of these modes can be made in general.

## 4 Non-Axisymmetric Perturbations, $m \neq 0$

In the case of non-axisymmetric perturbations one has to solve the full equation (18) in order to obtain the eigen-frequencies and make a judgment on the stability of the system. Some important properties of the eigen-frequency spectrum can be established prior to solving the problem:

1. The eigen-frequencies of non-axisymmetric modes may assume generally complex values.
2. In the complex  $\omega$ -plane the eigen-frequency spectrum is symmetric with respect to the line  $\text{Im } \omega = 0$ , that is if  $\omega$  is an eigen-frequency then its complex conjugate  $\omega^*$  is also eigen-frequency. The presence of complex conjugate pair in the eigenvalue spectrum indicates the instability of the equilibrium under consideration since one of these eigen-frequencies corresponds to the perturbation growing in time.
3. Eigen-functions  $u$  are generally complex.
4. There is no degeneracy in this case: each eigen-frequency corresponds to a different eigen-function.

Unlike the axisymmetric case, in the case of  $m \neq 0$  the Alfven resonances are not the lines any more. Instead they form two "resonance" zones in the

complex  $\omega$ -plane:

$$\min_{x \in [x_1, x_2]} (-\omega_A + m\Omega(x)) < \text{Re } \omega < \max_{x \in [x_1, x_2]} (-\omega_A + m\Omega(x)), \quad (23)$$

$$\min_{x \in [x_1, x_2]} (\omega_A + m\Omega(x)) < \text{Re } \omega < \max_{x \in [x_1, x_2]} (\omega_A + m\Omega(x)), \quad (24)$$

where the resonance condition  $\text{Re } \omega = \pm\omega_A + m\Omega(x)$  is satisfied for some point  $x \in [x_1, x_2]$ . As follows from our numerical analysis for each set of wave-numbers  $(m, k, n_r)$  there are four different eigen-frequencies. Two of them are always real (stable) and situated just outside the "resonance" zones, one in the left outer region with

$$\text{Re } \omega < \min_{x \in [x_1, x_2]} (-\omega_A + m\Omega(x)),$$

another one in the right outer region with

$$\text{Re } \omega > \max_{x \in [x_1, x_2]} (\omega_A + m\Omega(x)).$$

The other two eigen-frequencies lie either in the "inner" region between the resonances

$$\max_{x \in [x_1, x_2]} (-\omega_A + m\Omega(x)) < \text{Re } \omega < \min_{x \in [x_1, x_2]} (\omega_A + m\Omega(x)),$$

or in the "resonance" zones if these zones are overlapped. In former case the eigen-frequencies can be real or complex conjugate depending on the values of problem parameters. In latter case the eigen-frequencies are necessarily complex conjugate, that means the presence of instability.

As a typical example of non-axisymmetric eigen-frequency spectrum the spectrum for  $m = 1$  modes is shown in the figure 4. The resonance zones in this case are overlapped and all the "inner" eigen-frequencies are complex conjugate (due to the resolution of the figure 4 this fact is not so obvious for modes with the small imaginary parts of eigen-frequencies). In figure 5 samples of these unstable eigen-modes are presented.

Note that in the case of unstable mode with very small imaginary part of eigen-frequency a narrow singular layer is formed around the resonance point  $x_r$  defined by the condition

$$\text{Re } \omega = \pm\omega_A + m\Omega(x_r).$$

The eigen-function has the steep gradients in the neighborhood of this point (see Fig. 5b, 5c).

For the unstable non-axisymmetric mode the definition of its radial wave-number  $n_r$  is not so obvious as for axisymmetric one because the non-axisymmetric eigen-function is complex. We resolve this problem as follows: changing  $m$  continuously from its initial value to  $m = 0$  we find the corresponding axisymmetric mode with known  $n_r$ , this  $n_r$  is taken to be the radial wave-number of original non-axisymmetric mode. Although such definition is mathematically correct and non-ambiguous sometimes it leads to confusing results. For example, comparing the figures 5b and 5c one can see that both real and imaginary parts of eigen-function with  $n_r = 2$  have less number of zeros than the corresponding parts of eigen-function with  $n_r = 1$ .

Our main numerical results are related to the study of MRI growth rate (or increment,  $\gamma = \text{Im } \omega$ ) as a function of wave-numbers  $m, k, n_r$ . The figure 6 demonstrate the dependence of instability growth rate on the azimuthal wave-number  $m$  ( $m$  is used here as continuous parameter) for eigen-modes with different radial wave-numbers  $n_r$ . As one can see beginning with  $n_r = 1$  the system under consideration has a threshold of instability,  $m_{cr}$ , besides the value of  $m_{cr}$  is larger for larger  $n_r$ . If  $m > m_{cr}$  the eigen-mode with corresponding radial wave-number is always unstable, although the increment of instability decreases with growth of  $m$ . This fact contradicts to the local approach in which the unstable modes become stabilized with increasing values of  $m$  (see, for example, [11]). Also it is worth noting that the maximum possible value of the increment decreases with increase of radial wave-number  $n_r$ . In this sense the most unstable mode is the mode with the lowest radial wave-number,  $n_r = 0$ .

The figure 7 demonstrates the dependence of the increment  $\gamma$  on the azimuthal  $m$  and axial  $k$  wave-numbers for modes with  $n_r = 0$ . According to this dependence, for every value of  $m$  there exists a threshold value of axial wave-number  $k_{cr}(m)$  after which the eigen-mode with  $n_r = 0$  is always stable. This threshold value increases with growth of  $m$  and, as we believe, approaches the asymptote  $k_{cr} \propto m$  (the explanation is in the next section).

Dependencies of the increment on  $k$  for some  $m$  are shown in more details in figure 8. In fact, this figure represents the sections of the figure 7 at corresponding  $m$ .

Since the minimal axial wave-number  $k$  is determined by the height of the channel (see eq. 20) we conclude that choosing the height to be small enough (that is the minimal  $k$  is bigger than  $k_{cr}$ ) one can suppress the instabilities with low  $m$ . In particular, the situation is possible when there is instability for  $m = 1$  mode but there is no instability for axisymmetric  $m = 0$  mode.

## 5 Marginal Stability

As we have mentioned above *if the resonance zones in the complex  $\omega$ -plane are overlapped all the inner modes become unstable*. Although we checked this statement only for the small range of  $m$  (from 0 to 3) we believe that this is also true for larger  $m$ . Our limitations in  $m$  are related to the computer accuracy: in fact the growth rates for large  $m$  are so small that they can not be resolved in the code even by double float representation.

Accepting this statement as a hypothesis we obtain from conditions (23) and (24) that all inner modes (with any radial wave-number  $n_r$ ) become unstable if

$$\max_{x \in [x_1, x_2]} (m\Omega(x) - \omega_A) = \min_{x \in [x_1, x_2]} (m\Omega(x) + \omega_A).$$

Taking into account that  $x_1 = 1$  and the angular velocity profile is  $\Omega(x) = 1/x$ , we obtain

$$m - \omega_A = \frac{m}{x_2} + \omega_A,$$

which gives a critical value of axial wave-number  $k$  as a function of  $m$ :

$$k_{cr}(m) = \frac{m}{2v_A} \left( 1 - \frac{1}{x_2} \right). \quad (25)$$

It means that all "inner" modes (with any  $n_r$ ) become unstable if the axial wave-number  $k$  is less than the critical value defined by (25).

In reality the instability can occur for larger values of  $k$ , the actual marginal stability curves depend on the radial wave-number  $n_r$ . In the figure 9 the marginal stability curves calculated for  $n_r = 0$  and  $n_r = 1$  are shown. For comparison, the critical line  $k_{cr}(m)$  is also plotted. It is quite clear that this line is asymptote for both presented curves in the limit  $m \rightarrow \infty$ . Besides the critical line almost coincides with the marginal stability in the case of large radial wave-numbers,  $n_r \gg 1$ .

Note that the system under consideration has the only unstable axisymmetric mode with radial wave-number  $n_r = 0$ . All axisymmetric modes with  $n_r \geq 1$  are stable regardless of the value of  $k$ . From the figure 9 and expression (25) it also follows that in this system there are always non-axisymmetric eigen-modes which are spectrally unstable due to magnetorotational instability.

## 6 Conclusions

We have examined the spectral stability of electrically driven liquid metal flow in the model relevant to the new MRI experiment and presented a de-

tailed numerical analysis of eigen-functions and eigen-frequencies inherent in this model. The obtained results show that the rotation profile given by the expression (1) is always unstable due to MRI. For the chosen parameters of the experimental device the highest growth rate of instability  $\gamma$  corresponds to the axisymmetric mode  $m = 0$  with the lowest radial wave-number  $n_r = 0$ . Consequently, in the experiment with electrically driven flow one should expect the rapid excitation of axisymmetric magnetorotational instability. The modes with other wave-numbers are also presented but they are not so robust as the axisymmetric one.

From our analysis it turns out that the growth rate of axisymmetric MRI is quite sensitive to the device parameters. For example, choosing the height of the channel to be small enough (to make the smallest possible  $k$  in the system bigger than its threshold value for  $m = 0$ ) one can suppress the axisymmetric MRI while the unstable modes with  $m \neq 0$  will still exist.

The model which we have considered here is, of course, idealized. We did not take into account the dissipative effects (viscosity and resistivity) as well as the deviations of the equilibrium velocity from the profile given by the equation (1). These effects can change the conditions for MRI excitation in the experiment; they will be a subject of our future study.

We would like to acknowledge E. P. Velikhov for statement of this problem and V. P. Lakhin for useful discussions. This work is supported in part by NSERC Canada, NATO Collaboration Linkage Grant and Global Partners Award (University of Saskatchewan, Canada).

## References

- [1] E. P. Velikhov, *Sov. Phys. JETP* **36**, 995 (1959).
- [2] S. A. Balbus and J. F. Hawley, *Astrophys. J.* **376**, 214 (1991).
- [3] G. Rüdiger and Y. Zhang, *Astron. Astrophys.* **378**, 302 (2001).
- [4] H. T. Ji, J. Goodman, and A. Kageyama, *Mon. Not. R. Astron. Soc.* **325**, L1 (2001).
- [5] K. Noguchi, V. I. Pariev, S. A. Colgate, H. F. Beckley, and J. Nordhaus, *Astrophys. J.* **575**, 1151 (2002).
- [6] R. Hollerbach and G. Rüdiger, *Phys. Rev. Lett.* **95**, 124501 (2005).
- [7] K. Noguchi, V. I. Pariev, *astro-ph/0309340* (2003).

- [8] D. R. Sisan, N. Mujica, W. A. Tillotson, Y.-M. Huang, W. Dorland, A. B. Hassam, T. M. Antonsen, and D. P. Lathrop, *Phys. Rev. Lett.* **93**, 114502 (2004).
- [9] R. Hollerbach and A. Fournier, in *MHD Couette Flows: Experiments and Models*, edited by R. Rosner, G. Rüdiger, and A. Bonanno, AIP Conf. Proc. No. 733 (AIP, New York, 2004), p. 114.
- [10] I. V. Khalzov and A. I. Smolyakov, *Technical Physics* **51**, 26 (2006).
- [11] W.-T. Kim and E. C. Ostriker, *Astrophys. J.* **540**, 372 (2000).
- [12] C. Curry, R. E. Pudritz, and P. G. Sutherland, *Astrophys. J.* **434**, 206 (1994).
- [13] C. Curry and R. E. Pudritz, *Mon. Not. R. Astron. Soc.* **281**, 119 (1996).
- [14] G. Rüdiger, M. Schultz, and D. Shalybkov, *Phys. Rev. E* **67**, 046312 (2003).
- [15] J. Goodman and H. Ji, *J. Fluid Mech.* **462**, 365 (2002).
- [16] E. A. Frieman and M. Rotenberg, *Rev. Mod. Phys.* **32**, 898 (1960).
- [17] G. I. Ogilvie and J. E. Pringle, *Mon. Not. R. Astron. Soc.* **279**, 152 (1996).
- [18] R. Keppens, F. Casse, and J. P. Goedbloed, *Astrophys. J.* **569**, L121, (2002).

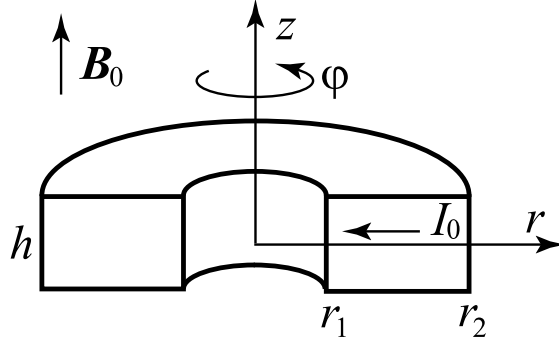


Figure 1: Geometry of the electrically driven flow for MRI study.

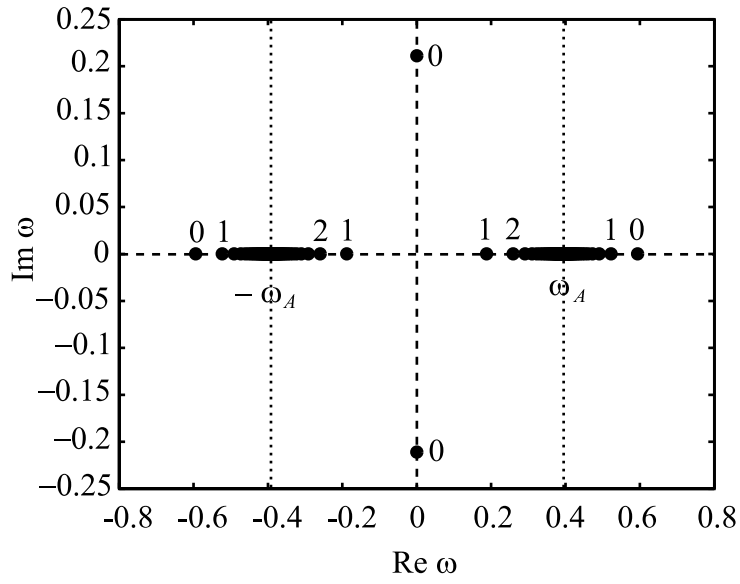


Figure 2: Eigen-frequency spectrum in case  $m = 0$ ,  $k = \pi/2$ . Dashed lines represent real and imaginary axes, dotted lines correspond to Alfvén resonances. Radial wave-numbers  $n_r$  are shown for some modes.

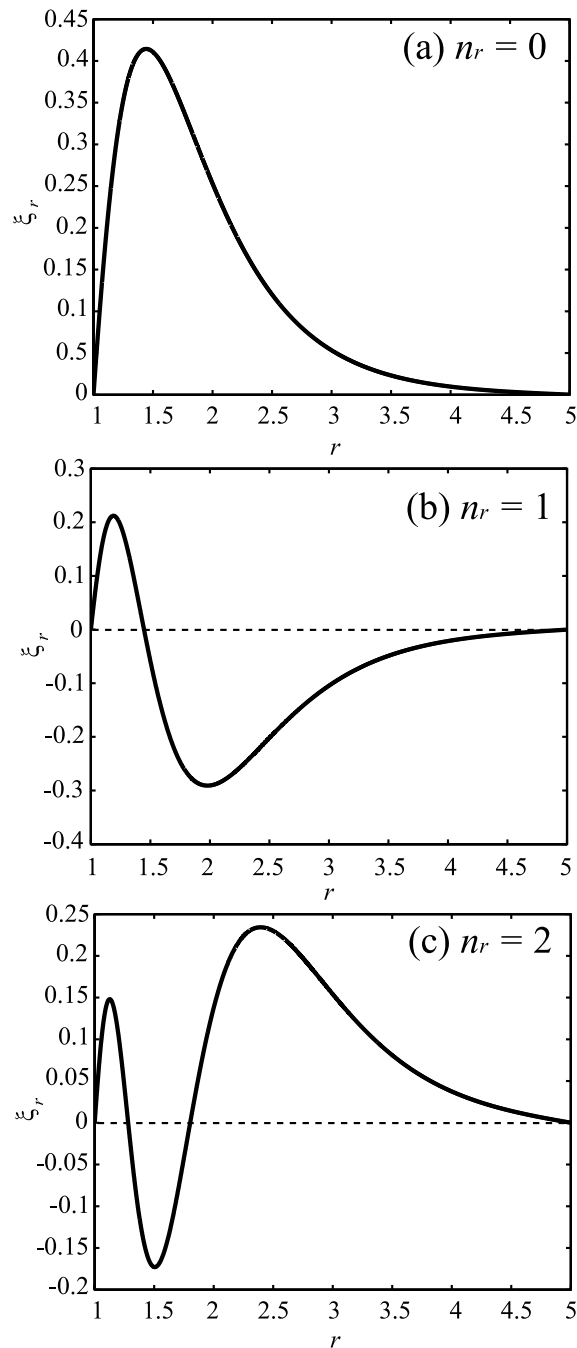


Figure 3: Eigen-functions in case  $m = 0$ ,  $k = \pi/2$ . Corresponding radial wave-numbers and eigen-frequencies are (a)  $n_r = 0$ ,  $\omega = \pm 0.2099i$ ,  $\pm 0.5937$ ; (b)  $n_r = 1$ ,  $\omega = \pm 0.1908$ ,  $\pm 0.5216$ ; (c)  $n_r = 2$ ,  $\omega = \pm 0.2625$ ,  $\pm 0.4894$ .



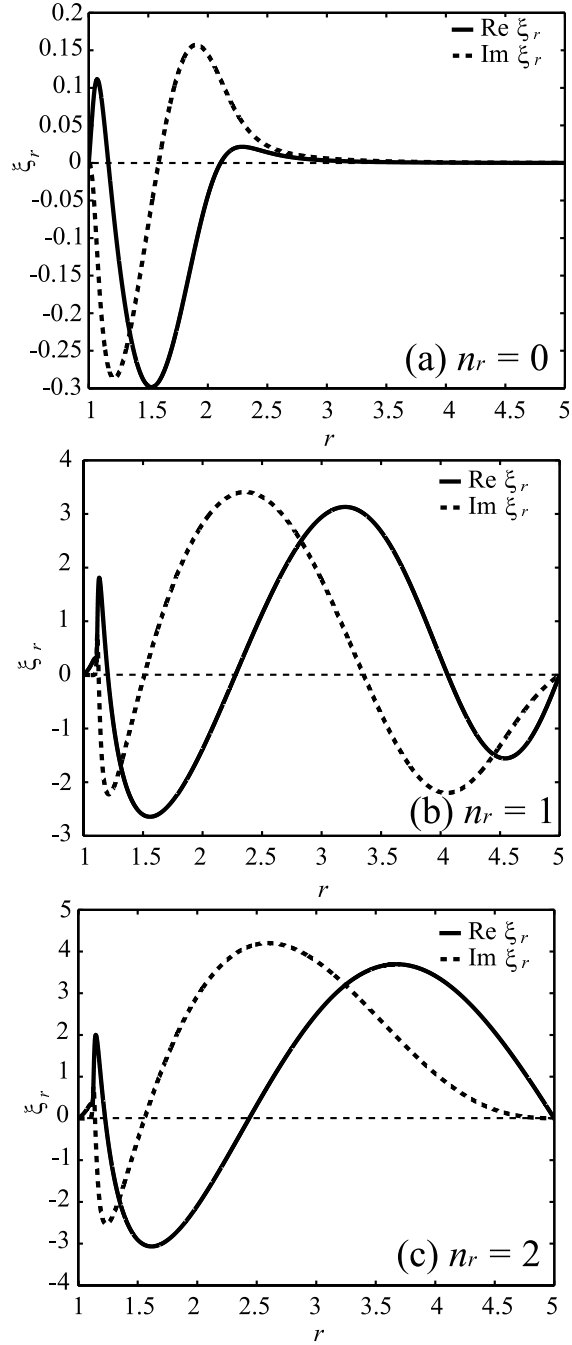


Figure 5: Eigen-functions in case  $m = 1, k = \pi/2$ . Real (solid) and imaginary (dashed) parts are shown. Corresponding radial wave-numbers and eigen-frequencies are (a)  $n_r = 0, \omega = 0.5623 + 0.0791i$ ; (b)  $n_r = 1, \omega = 0.4173 + 0.0073i$ ; (c)  $n_r = 2, \omega = 0.3994 + 0.0093i$ .

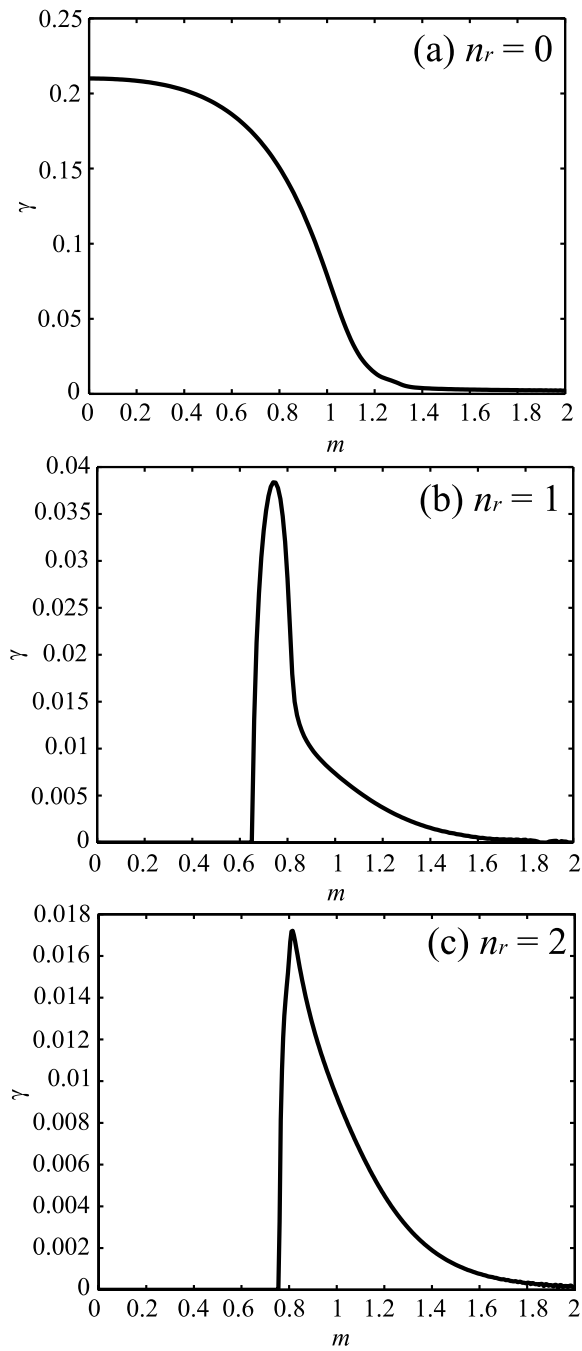


Figure 6: Growth rate dependence on azimuthal wave-number  $m$  in case  $k = \pi/2$ : (a)  $n_r = 0$ ; (b)  $n_r = 1$ ; (c)  $n_r = 2$ .

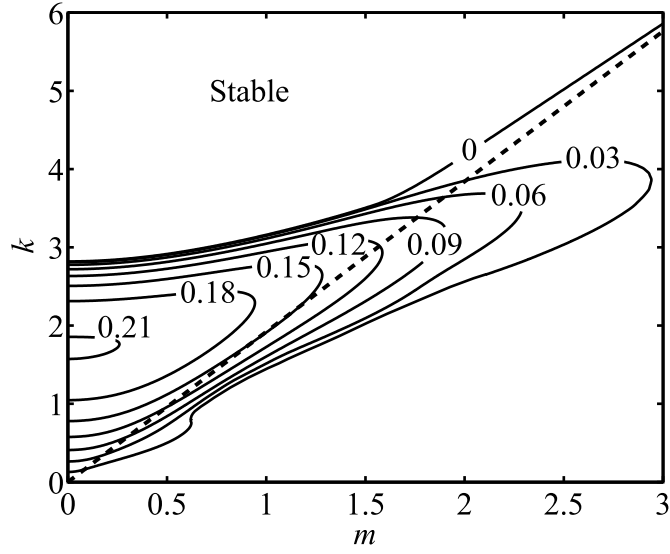


Figure 7: Growth rate dependence on azimuthal  $m$  and axial  $k$  wave-numbers in case  $n_r = 0$ . Solid contours show the levels of function  $\gamma(m, k)$ . The dashed line is the asymptote for the contour  $\gamma(m, k) = 0$ .

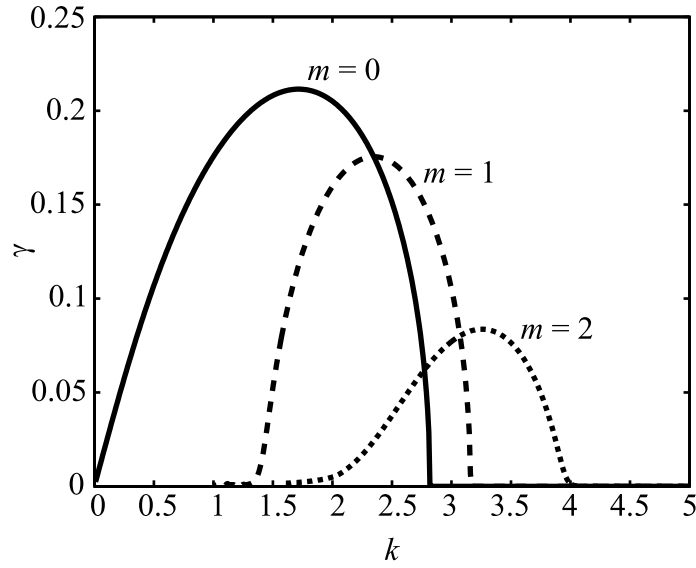


Figure 8: Growth rate dependence on axial wave-number  $k$  for different  $m$  in case  $n_r = 0$ . Solid line is for  $m = 0$ , dashed – for  $m = 1$ , dotted – for  $m = 2$ .

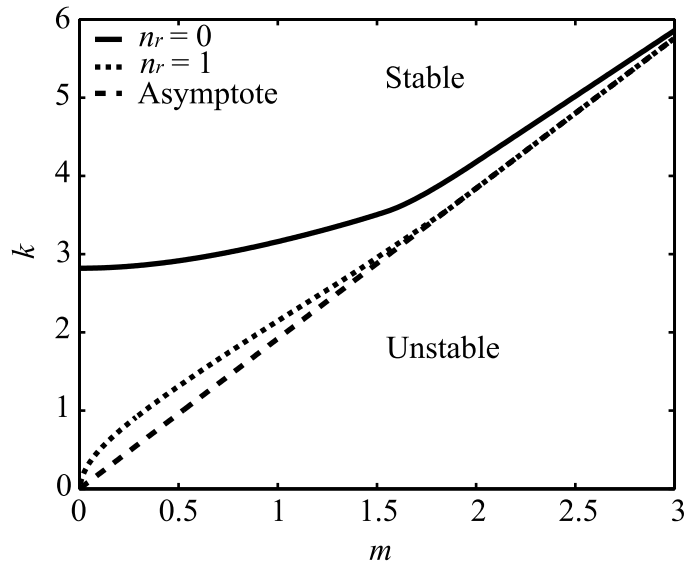


Figure 9: Marginal stability in  $(k, m)$ -plane for different radial wave-numbers  $n_r = 0$ . Solid line is for  $n_r = 0$ , dotted – for  $n_r = 1$ ; dashed line is their asymptote.